

The Halos and Environments of Nearby Galaxies (HERON) Survey IV: Complexity in the boxy galaxies NGC 720 and NGC 2768

Andreas J. Koch-Hansen¹, Anna Pasquali¹, R. Michael Rich², Ortwin Gerhard³, and Oliver Müller⁴

¹ Zentrum für Astronomie der Universität Heidelberg, Astronomisches Rechen-Institut, Mönchhofstr. 12, 69120 Heidelberg, Germany; e-mail: andreas.koch@uni-heidelberg.de

² University of California Los Angeles, Department of Physics & Astronomy, Los Angeles, CA, USA

³ Max-Planck-Institut für Extraterrestrische Physik, Gießenbachstraße 1, 85748 Garching, Germany

⁴ Institute of Physics, Laboratory of Astrophysics, Ecole Polytechnique Fédérale de Lausanne (EPFL), 1290 Sauverny, Switzerland

ABSTRACT

The shapes of galaxies, in particular their outer regions, are important guideposts to their formation and evolution. Here we report on the discovery of strongly box-shaped morphologies of the, otherwise well-studied, elliptical and lenticular galaxies NGC 720 and NGC 2768 from deep imaging. The boxiness is strongly manifested in the shape parameter A_4/a of -0.04 in both objects, and also significant center shifts of the isophotes of $\sim 2-4$ kpc are seen. One reason for such asymmetries commonly stated in the literature is a merger origin, although the number of such cases is still sparse and the exact properties of the individual boxy objects is highly diverse. Indeed, for NGC 2768, we identify a progenitor candidate (dubbed *Pelops*) in the residual images, which appears to be a dwarf satellite that is currently merging with NGC 2768. At its absolute magnitude of M_r of -12.2 mag, the corresponding Sersic radius of 2.4 kpc is more extended than those of typical dwarf galaxies from the literature. However, systematically larger radii are known to occur in systems that are in tidal disruption. This finding is bolstered by the presence of a tentative tidal stream feature on archival GALEX data. Finally, further structures in the fascinating host galaxy comprise rich dust lanes and a vestigial X-shaped bulge component.

Key words. Galaxies: formation — Galaxies: halos — Galaxies: individual: NGC 720, NGC 2768 — Galaxies: interactions — Galaxies: elliptical and lenticular, cD — Galaxies: structure

1. Introduction

The morphology of galaxies holds important clues about their formation and evolutionary processes, be it in the spiral-vs-elliptical dichotomy, prominently illustrated in the Hubble tuning fork and its extensions (Hubble 1926; de Vaucouleurs 1959), or via including irregular objects that often are the result of past or ongoing tidal interactions or mergers (Arp 1966; Tal et al. 2009).

One particular case are galaxies with isophotes that significantly deviate from smooth ellipses¹. The most extreme deviations can tend towards a “disky” ($A_4/a > 0$) or a “boxy” ($A_4/a < 0$) shape. Graham et al. (2012) report on a rectangular dwarf galaxy (LEDA 074886; $M_R = -17.3$ mag) with a very high negative boxiness parameter ranging from $A_4/a = -0.05$ to -0.08 between 3 and 5 kpc, which they dubbed the “Emerald Cut Galaxy” (in the following “ECG”). One possible reason for the ECG’s boxiness discussed in their work is the edge-on merger of two spiral galaxies. However, Graham et al. (2012) emphasize that there are only a few highly boxy examples known in the literature, yet the details of their shapes are diverse, and accordingly pinning down one single formation channel is unrealistic.

¹ Commonly quantified in terms of the fourth-order Fourier parameter in an isophote analysis. The nomenclature of these parameters differs amongst the literature. Here, we follow the internal naming of our used IRAF *ellipse* task, which denotes the isophote-intensity weighted fourth moment (B_4/a) as A_4/a (e.g., Bender & Moellenhoff 1987; Jedrzejewski 1987; Bender et al. 1988, 1989) and similar for the third moments ($B_3/a \equiv A_3/a$).

This picture has hardly changed in the literature over the past decade.

Here, we report on the discovery of boxy morphologies in the halo of two, otherwise well-studied, galaxies in the Local Volume: NGC 720 (E5) and 2768 (E6/S0), each with stellar masses of a few $\times 10^{11} M_\odot$ (Rembold et al. 2005; Forbes et al. 2012; Pastorello et al. 2014). Rich et al. (2019) lists their halo shape as “boxy” and “round”, respectively, purely based on visual inspection. Prompted by previous, shallower works that did not detect any peculiarities in these objects, this begs the question of whether their boxiness is an intrinsic property of the individual galaxy or if it might represent the general presence of disks or other substructures (e.g., Pasquali et al. 2007). To this end, we employ new deep imaging from the “Halos and Environments of Nearby Galaxies” (HERON) survey (Rich et al. 2019), bolstered by archival data from the Sloan Digital Sky Survey (SDSS), and the Galaxy Evolution Explorer (GALEX; Bianchi & GALEX Team 2000; Morrissey et al. 2007) to investigate the shapes of those two particularly boxy galaxies. This paper is organized as follows: in Sect. 2, we describe the images that are the basis of our study. Sect. 3 is dedicated to the structural analysis of the two galaxies. Finally, we discuss our findings in terms of the formation histories of either object in Sect. 4.

2. Observations: Centurion 28 imaging

Out of the sample of 119 HERON galaxies the two objects of this study were chosen by eye based on their optical appearance and

indications of boxiness. In the following, we briefly introduce the two data sets employed in our structural analysis.

The images used in this work were taken as part of the HERON survey and details of their reduction are given in Rich et al. (2019), alongside a general characterization of the galaxies, for instance in terms of their halo sizes. Imaging for the two targets was acquired in Oct. and Nov. 2011 with the 28-inch Centurion (C28) telescope at the Polaris Observatory Association in Lockwood Valley, California (Rich et al. 2012; Brosch et al. 2015; Koch et al. 2017; Rich et al. 2019). The pixel scale of the detector is $0.82'' \text{ pixel}^{-1}$, which for NGC 720 has been re-sampled by a factor of two in either dimension. This corresponds to 218 and 88 pc per pixel at the adopted distances of NGC 720 and 2768, respectively².

The fields around the galaxies were exposed for 13×300 s (NGC 720) and 3×300 s (NGC 2768) using a broad-band Astrodon Luminance filter, which has a bandwidth from 4000 to 7000 Å and thus effectively acts as a wide Sloan *r*-filter. As a result, the images reach surface brightnesses of 29.9 and 28.9 $\text{mag sq. arcsec}^{-1}$ for NGC 720 and NGC 2768, respectively. The seeing conditions of the observations were rather low, at $6.4''$ for NGC 720 and $3.5''$ for NGC 2768. Fig. 1 shows the full C28 images for either galaxy.

The fundamental coordinate system was attached to the images using the public service *astrometry.net* (Lang et al. 2010), which builds on blind pattern matching. Finally, we obtained the photometric calibration by performing aperture photometry of stellar sources within the images using SExtractor (Bertin & Arnouts 1996), and cross-matching the results to the *r*-band photometry of the 14th data release of the Sloan Digital Sky Survey (SDSS DR14; Abolfathi et al. 2018).

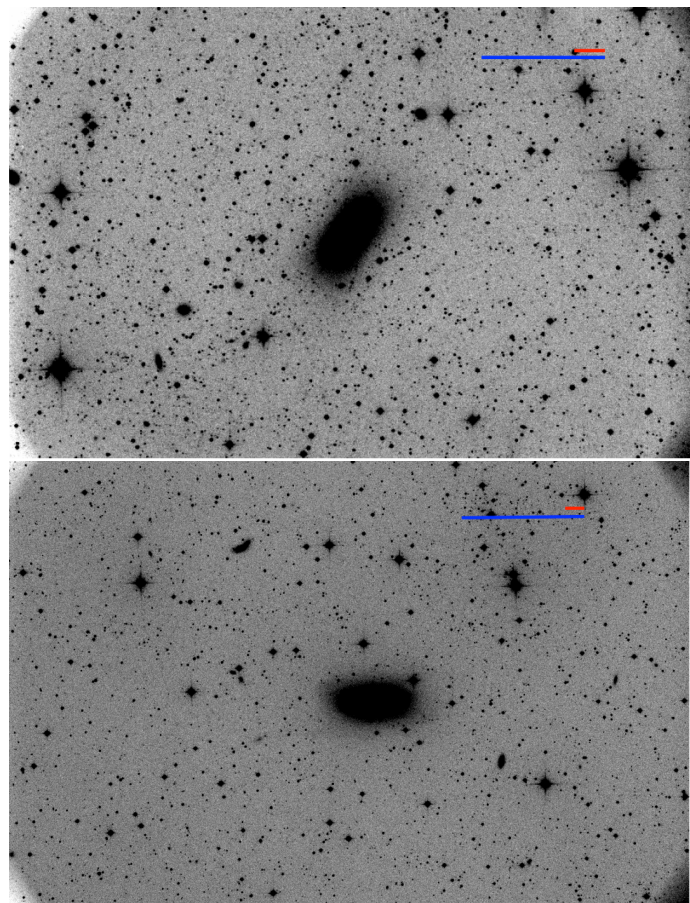


Fig. 1. Full C28 images of NGC 720 (top panel) and NGC 2768 (bottom panel) on a linear stretch. North is up, East is left. We also indicate scale bars of $10'$ (blue line) and 20 kpc (red line) at the adopted distance to the galaxies.

3. Analysis

We performed an isophotal analysis of both galaxies using IRAF's *ellipse* task (as was also done by Graham et al. 2012), which fits basic ellipse parameters to the flux, with the option to include higher order parameters, where our chief focus lies on A_4/a . To prepare the images, stellar sources were masked within IRAF and we used a 2σ -clipping within *ellipse* to interpolate over any possible residual flux. The resulting radial profiles of the key shape parameters are shown in Figs. 2 and 4 for either galaxy down to 3σ above the sky, and in the following we discuss the implications for their boxiness and potential formation scenarios. For the case of the surface brightness profile, the magnitudes have been corrected for extinction by $A_r = 0.036 \text{ mag}$ for NGC 720 and $A_r = 0.103 \text{ mag}$ for NGC 2768 (Schlafly & Finkbeiner 2011).

3.1. NGC 720

In the first series of HERON papers, Rich et al. (2019) traced NGC 720 down to a surface brightness of $29.9 \text{ mag arcsec}^{-2}$ and stated a halo diameter at a flat-rate $28.0 \text{ mag arcsec}^{-2}$ by ocular inspection. The respective halo “size” thus extends to 23 times its half-light radius (at 6.7 kpc), and the profile sampled in this work reaches to about 10 half-light radii. We note, however, that our profiles are truncated at a surface brightness of 3σ above the background. NGC 720 has been classified as an E5 galaxy with a total mass of $3.29 \times 10^{11} M_\odot$ (Rembold et al. 2005) and only

² The distances were taken as 27.38 Mpc and 22.15 Mpc to NGC 720 and NGC 2768, respectively (see Rich et al. 2019 and references therein).

little rotation. Also our ellipticity profile (middle left of Fig. 2) meanders around the corresponding value of $\epsilon \sim 0.4\text{--}0.6$.

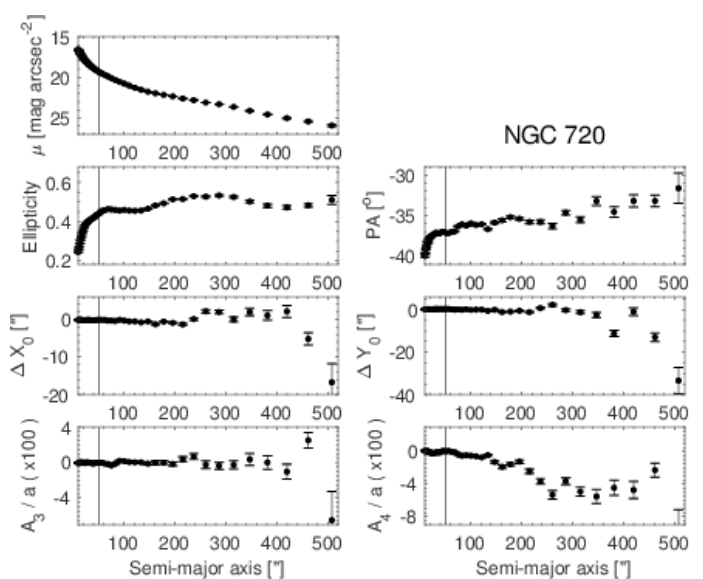


Fig. 2. Photometric and morphological parameters of NGC 720 from *ellipse*, shown as a function of semi-major axis distance. The half-light radius is indicated.

Of main interest for our present work is the intensity-weighted mean boxi-/diskiness parameter A_4/a . This is typically measured from 2 seeing radii to 1.5 half-light radii (e.g., Carter 1978, 1987; Bender et al. 1989; Hao et al. 2006; Graham et al. 2012). To guide the eye, galaxies that are labelled “boxy” (excluding dwarfs) have parameters ranging from -0.02 to around zero, with values reported as low as -0.04 (e.g., Hao et al. 2006). The boxiness parameters around -0.04 are effectively rare in the literature. Here, the ECG stands out in having very low values of -0.05 down to -0.08 between 3 and 5 kpc (Graham et al. 2012). The boxy nature of NGC 720 has already been noted by Rich et al. (2019) “by eye” and is now quantitatively confirmed (bottom left panel of Fig. 2), reaching an A_4/a of -0.04 in its outskirts, which uniquely classifies this galaxy as a boxy one, albeit to a lesser extent than the ECG.

Moreover, we find a strongly varying center position for NGC 720 throughout the annuli, varying by 10–20 px (~ 2 –4 kpc at the adopted distance). This is likely due to the same event that caused the boxiness of the isophotes, which we conjecture to be a merger (see also Sect. 3.2.2). The residual image (Fig. 3) displays further butterfly-shaped features, which are a common feature if the disk component is not properly modelled and removed, thus revealing complexities in the disk such as dust lanes.

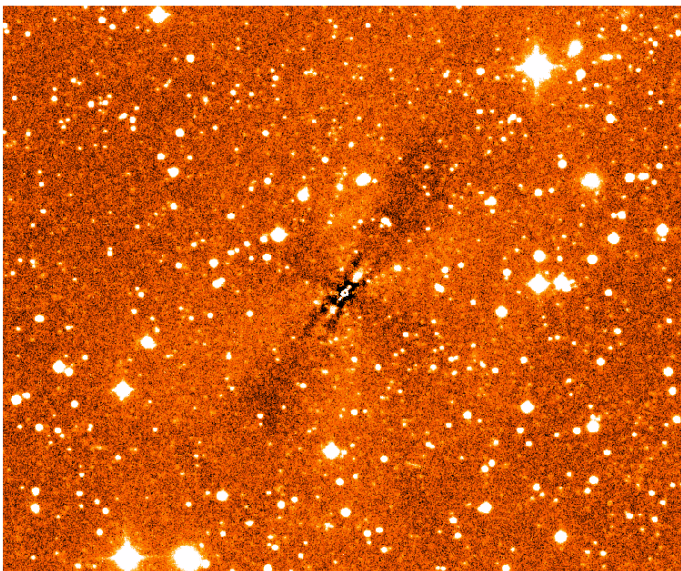


Fig. 3. Model subtracted image of NGC 720, covering $25' \times 20'$. North is up, East is left.

3.2. NGC 2768

This galaxy has been traced down to $28.9 \text{ mag arcsec}^{-2}$ by Rich et al. (2019) and its diameter at the $28 \text{ mag arcsec}^{-2}$ level is reported as 96 kpc, corresponding to ~ 13 effective radii (the latter being 7.6 kpc). In turn, the data under scrutiny here cover approximately six half-light radii (above 3σ of the sky) before the background hampered a further meaningful analysis. NGC 2768 already appears boxy to the eye (Fig. 1), which is bolstered by the shape profiles in Fig. 4 (bottom right panel). The low values of A_4/a of -0.04 in its outer regions render it a clear contender for a boxy galaxy. Its nature as a purported lenticular to elliptical (E5) galaxy is also sustained by our derived ellipticity profile (middle left panel of Fig. 4). As for NGC 720, we find a significant center shift across the full isophotes, amounting to as much

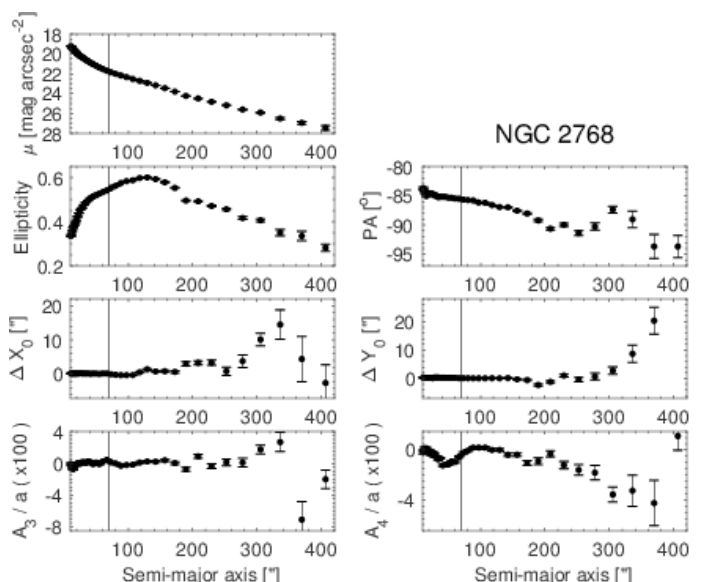


Fig. 4. Same as Fig. 2, but for NGC 2768.

as 20 px in x and y -direction, which corresponds to ~ 1.8 kpc at the used pixel scale and adopted distance to the target galaxy. In fact, the most pronounced shifts for both galaxies, appears after 200–300 arcsec.

A hint of the peculiarity in this galaxy was already found by Pulsoni et al. (2018), who measured the kinematics of planetary nebulae out to $5 R_e$, resulting in a non-point-symmetric distribution. They found this object to be a fast rotator out to large radii, and they quantified its asymmetry with similar parameters to ours (viz., c_4 and s_4 , accounting for sine and cosine projections). Pulsoni et al. (2018) judged these asymmetries as “likely real” as they have also already been seen in the deep optical images of Duc et al. (2015).

3.2.1. A disk in NGC 2768

A prominent dust lane, as visible as black stripes on the model-subtracted image of NGC 2768 (Fig. 5), had already been noted by Kim (1989) and a hint of it can also be seen on our original C28 image (Fig. 1) when using a proper stretch. Moreover, we note the possible presence of a vestigial x-shaped bulge structure as is also known to exist in the Milky Way (McWilliam & Zoccali 2010). An identical isophotal analysis on the HST data

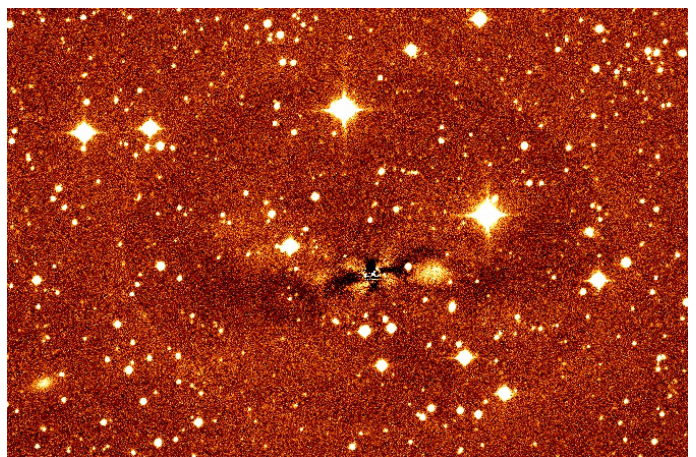


Fig. 5. Model subtracted image of NGC 2768, covering $20' \times 13'$.

as on our C28 imaging reveals the exact same features. Finally, we note that we have also investigated archival SDSS images in the r -band, which confirm the presence of the dust.

3.2.2. The progenitor that built NGC 2768

Fig. 6 is the result of masking not only the stars before running *ellipse*, but also masking the dust features mentioned in Sect. 3.2.1. This model subtracted image clearly shows the presence of a large plume towards the West of NGC 2768's center, which we consider to be the ongoing merger that caused the strong distortions of NGC 2768's isophotes, which we henceforth dub *Pelops*³. Using *GALFIT* (Peng et al. 2002) we fitted a Sersic-profile to the model-subtracted image. The result of this fit is shown in Fig. 6 and its basic parameters are summarized in Table 1. *GALFIT* explicitly accounts for the point spread function (PSF) of the images in its fitting so that the stated radii are the ones obtained after deconvolution with the PSF profile. Similarly, this is considered (internally within *GALFIT*) for the error analysis.

Table 1. Parameters of the NGC 2768 merger candidate, *Pelops*.

Parameter	Value	Method ^a
α	09:11:24.6	G, C28
δ	+60:02:18.2	G, C28
M_R	-12.2 ± 0.2	G, C28
μ_e	22.96 ± 0.01	G, C28
r_e	2.4 ± 0.3 kpc	G, C28
n	0.37 ± 0.02	G, C28
e	0.55 ± 0.01	G, C28
P.A.	$88.4^\circ \pm 1.1^\circ$	G, C28
u_0	19.19 ± 0.26	A, SDSS
g_0	17.93 ± 0.14	A, SDSS
r_0	17.00 ± 0.09	A, SDSS
i_0	16.65 ± 0.08	A, SDSS
z_0	16.50 ± 0.07	A, SDSS
$(g-r)_0$	0.93 ± 0.17	D
$(r-i)_0$	0.35 ± 0.12	D

Notes. ^(a) G, C28: *GALFIT* values from our C28 images; A, SDSS: Aperture photometry within r_e on the SDSS residual images; D: Derived

Assuming this blob feature (Casey et al. 2023) to be at the same distance as NGC 2768, we determine its absolute magnitude as $M_r = -12.2 \pm 0.12$ mag. The best-fit Sersic index was determined as 0.37 ± 0.02 , which is rather small and typical of disrupting galaxies and indicates that a simple Sersic-modeling is not adequate anymore. Furthermore, we determine an axis ratio of 0.55 ± 0.01 and the position angle of *Pelops* of $88.4^\circ \pm 1.09^\circ$. To find further evidence of the reality of the merging galaxy, we consulted archival data from the Galaxy Evolution Explorer (GALEX; Bianchi & GALEX Team 2000; Morrissey et al. 2007), which targeted the surroundings of NGC 2768 in the context of the NGA campaign (Gil de Paz et al. 2007) in Feb. 2005. While no detection can be made in the Far-ultraviolet (UV) image, the 182-s exposure in the Near-UV clearly depicts the host galaxy (Fig. 7). Furthermore, we note the presence of a vestigial stream and possibly an extension into a further arc to the South of the host galaxy. These are indicated by eye in the

³ Son of Tantalos. According to Greek mythology, Pelops was "tidally disrupted" (rather, chopped to pieces) to feast the Gods.

bottom panel of Fig. 7. A natural suspicion is that the structure we see could be a reflection. However, according to the GALEX documentation⁴, ghosts chiefly appear at 30–60'' above and below the bright source along the y -direction on the detector. In our case, the arcs appear at a much larger separation of 140'' with an even larger extent and a shape that does not resemble the ghostly donut-shapes. Therefore, we deem it unlikely, that the purported stream is an artefact.

3.2.3. Properties of *Pelops* from SDSS images

The same feature also stands out in identically model-subtracted SDSS images in the g , r , and i -bands, confirming that we are most likely seen a real feature, while being fainter in the u - and z -bands. The (lack of) depth of the SDSS prevents us from obtaining any meaningful structural or photometric parameters from *GALFIT*. However, we performed *aperture* photometry by simply adding the calibrated flux on each image within one effective radius, both of the merger candidate and of the host galaxy. The magnitudes were dereddened using the dust maps of Schlafly & Finkbeiner (2011) and the extinction law of Cardelli et al. (1989). Here, it worth noticing that both the $g-r$ and $r-i$ colours of both objects are in very good agreement to within the (Poisson) errors.

Based on our photometry, we consulted the E-MILES simple stellar population (SSP) models (Vazdekis et al. 2016), which we computed for a LMC-like metallicity and with the universal initial mass function of Kroupa (2001) for 53 ages between 0.03 Gyr and 14 Gyr. For each age, we varied the *intrinsic* reddening, A_V , between 0 and 2 in steps of 0.05. Next, we computed the reduced χ^2_ν between the predicted SSP colours and the ones measured from the SDSS images. This results in a best-fit age of $6.5^{+5.5}_{-3.8}$ Gyr and an intrinsic reddening of 0.15 ± 0.15 mag. The according mass-to-light (M/L) ratio in the r -band is found to be $1.9^{+1.0}_{-0.9}$ in Solar units, which is rather on the low side for a typical dwarf galaxy (e.g., Koch 2009). This would imply, adopting the satellite's absolute magnitude, a total mass of $\sim 10^7 M_\odot$.

3.2.4. *Pelops* in context

The surface brightness at the effective radius is fully in agreement with those of dwarf galaxies in various environments (Fig. 8, middle panel). However, at its absolute magnitude this merging candidate appears too large by a factor of a few, when compared to typical galaxies of similar magnitude. Its corresponding half-light radius is 2.4 ± 0.3 kpc, and an investigation of systematically more extended objects is often used to confirm the presence and absence of tidal disruptions (Koch et al. 2017). Indeed, the contender within NGC 2768 lies within ± 1.5 mag of the strongly disrupted NGC 4449B (Rich et al. 2012) and HCC-087 (Koch et al. 2012) at similarly large radii. We note, however, that the shown literature sample is given in the Johnson-Cousins R-band (and in parts transformed from Sloan g - and i -band magnitudes; Byun et al. 2020), whereas our value is in Sloan- r and converted from our luminance measurement so that a slight offset in magnitude can be inherent. We further note that we adopted a single Sersic profile, which does not account for tidal features, while other galaxies in the literature may employ other types of profiles, adding to the discrepancy. Two data points in the bottom panel Fig. 8 are worth mentioning: firstly, the Local Group dwarf spheroidal And XIX, which, at

⁴ http://www.galex.caltech.edu/wiki/Public:Documentation/Chapter_8#Ghosts

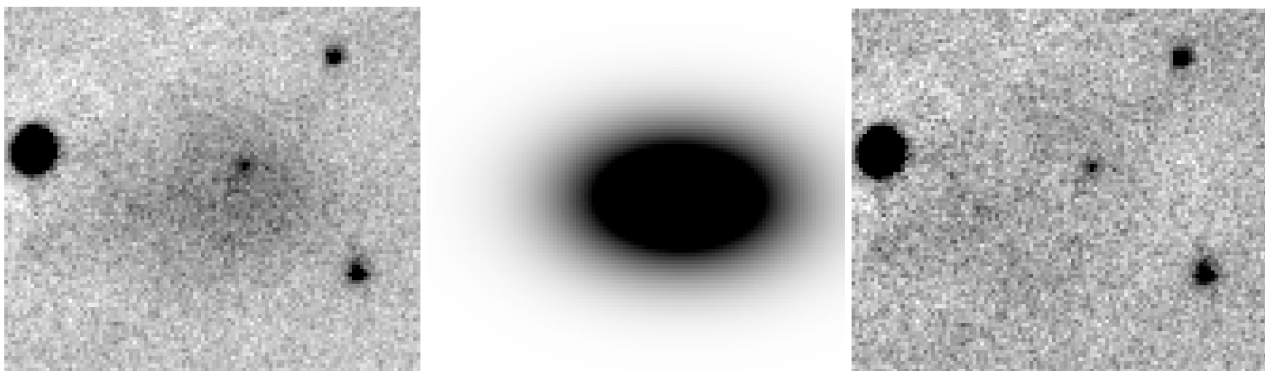


Fig. 6. Left panel: a $1.5' \times 1.3'$ image (thus encompassing ~ 4 half-light radii) centered on *Pelops*. The middle panel shows the best-fit ($\chi^2/\nu=0.96$) *GALFIT*-model, and the right panel depicts the residual image.

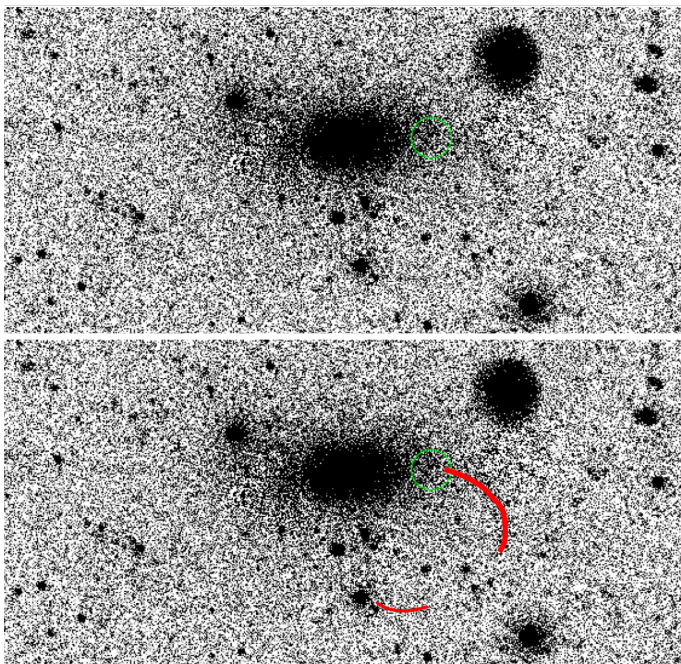


Fig. 7. GALEX NUV image of NGC 2768. The location of the *Pelops* overdensity identified in Fig. 6 is indicated with a green circle. The purported stream is highlighted by the red lines in the bottom panel. The image covers $14' \times 7'$.

$M_R = -9.74$ and $R_h = 1.7$ kpc (McConnachie 2012), stands out in the radius-magnitude diagram. Also this ultra-diffuse object is a result of tidal interactions with its host galaxy, M31 (Collins et al. 2020). Secondly, Antlia 2 has been named “an enormous Galactic dwarf satellite” (Torrealba et al. 2019), the properties of which are also indicative of a strong tidal evolution. We therefore conclude that the overdensity is, by effective and absolute magnitude, a common dwarf galaxy in the process of tidal interactions with the host, NGC 2768.

To place the merging galaxy in context, we compared its absolute magnitude with the Local Group dwarf sample (McConnachie 2012). Albeit given in the V-band, the satellite to NGC 2768 appears similar to Andromeda II, which, intriguingly, might be the remnant of a merger in itself (Amorisco et al. 2014). Our candidate has a luminosity of $\sim 5 \times 10^6 L_\odot$. Adopting the M/L-ratio determined above, this results in a mass of the dwarf candidate on the order of $10^7 M_\odot$. If the NGC 2768 merger and And II were of similar type and the present object had the same mass-to-light-ratio as And II (~ 20 Côté et al. 1999) this

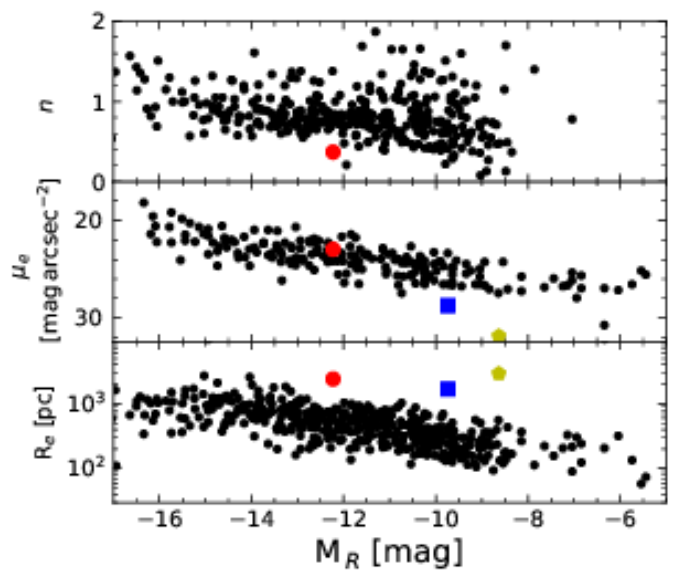


Fig. 8. Location of *Pelops* (red point) on the magnitude-radius plot (bottom panel) and in relation with the surface brightness at effective radius (middle panel) and the Sersic-index (top panel). Data from dwarf galaxies in various groups and clusters are shown as black points (Chiboucas et al. 2009; Müller et al. 2015; McConnachie 2012; Muñoz et al. 2015; Park et al. 2017; Byun et al. 2020). Indicated in blue and green are the dwarf spheroidals And XIX and Antlia 2, which are the most extended objects in the Local Group.

would yield a mass ten times larger, $\sim 10^8 M_\odot$. This compares to the host galaxy’s (disk plus bulge) mass of $\sim 10^{11} M_\odot$ (Forbes et al. 2012). No matter which M/L is used, we are thus facing a minor merger, which is still seemingly capable of deforming the structure of the galaxy and inducing many of its morphological and dynamical properties.

4. Discussion

Upon visual inspection of the rich HERON dataset, we detected unusually boxy isophotes of two, otherwise well-studied, galaxies. Such objects are hitherto rare, and in one case we could even identify a merger candidate, which we believe has caused the isophotal distortions.

Graham et al. (2012) suggested an edge-on merger of two disk galaxies as the origin of the ECG, one of the most rectan-

gular galaxies known. In their scenario, initial gas was driven inwards and formed an inner disk, while larger radii experienced a dissipationless merger. The “boxiness” parameters of the two well-known objects measured in our study are not as extreme as for the ECG (A_4/a of -0.08 vs. our -0.04). While no remnant could be identified for NGC 720, a merger origin of its morphology is bolstered by Rembold et al. (2005), who identified this galaxy as an unequal-mass merger remnant based on its kinematics from longslit spectroscopy.

NGC 2768 has been classified as an E5 galaxy (Pastorello et al. 2014), but has also been named E6/S0 (Zanatta et al. 2018; Rich et al. 2019). Already early on, it was found that its gas has different kinematics from the stars in the inner regions (Fried & Illingworth 1994), hinting at a dynamically special history. Similarly, Forbes et al. (2012) performed a bulge/disk decomposition based on various photometric and kinematic tracers (planetary nebulae, stars, and globular clusters) and found that the disk of NGC 2768 rotates rapidly, with its velocity dispersion decreasing with radius. In contrast, the bulge turned out to be pressure supported with only a slow rotation. As the resulting ratio of the disk’s rotational velocity to its velocity dispersion resembles that of a spiral galaxy, Forbes et al. (2012) conclude that NGC 2768 is a transformed late-type galaxy. Similarly, Zanatta et al. (2018), also using globular clusters and planetary nebulae as tracers, note that NGC 2768’s red (i.e., old) globular cluster system displays rotation, most pronounced at inner radii ($R < 1$ kpc), indicating that mergers seem to have played an important role. Overall, lenticular galaxies can evolve from spiral galaxies via various processes that remove most of their gas and erase spiral structures (e.g., Byrd & Valtonen 1990; Bournaud et al. 2005; Zanatta et al. 2018). Interestingly, also the ECG shows a disk-bar like structure in its very center, where a solid body rotation indicates the presence of a central disk (Forbes et al. 2011; Graham et al. 2012).

An obvious question is how frequent galaxies with such strongly boxy morphologies are in the (Local) Universe. Several similar contenders are reported in the literature (see Graham et al. 2012 and references therein), although none of them display such a boxiness as the ECG. For instance, Bidaran et al. (2020) find boxy isophotes in the Virgo cluster dE galaxy VCC 0608, which also has a severe misalignment between the photometric and kinematic position angles, indicative of a past merger. As Graham et al. (2012) discuss, all boxy galaxies have very individually different properties. Here, different galaxy types are covered, and head-tail structures and warps have also been identified. As a result, it remains difficult to uniquely identify one tailor-made mechanism to produce boxy isophotes.

Hao et al. (2006) reported that only 19 out of 847 (i.e., 2.2%) in their sample of nearby early-type galaxies (elliptical and lenticular) from the SDSS are boxy, with $-0.02 < A_4/a < -0.01$, while the remaining 97.8% show disky isophotes, i.e. $A_4/a > -0.01$. This fraction is in agreement with the number of boxy early-type galaxies in the Virgo Cluster Catalog (Binggeli et al. 1985, VCC) as identified in Graham et al. (2012) and Bidaran et al. (2020), which add up to $\sim 3\%$ the VCC’s population. This highlights that boxy galaxies are still a rare species that await further detections and require more in-depth investigations.

Acknowledgements. We thank the anonymous referee for a constructive report. The authors warmly thank W. Byun for sharing his data on dwarf galaxies. AJKH and AP gratefully acknowledge funding by the Deutsche Forschungsgemeinschaft (DFG, German Research Foundation) – Project-ID 138713538 – SFB 881 (“The Milky Way System”), subprojects A03, A05, A11, B05. OM is grateful

to the Swiss National Science Foundation for financial support under the grant number PZ00P2_202104.

References

- Abolfathi, B., Aguado, D. S., Aguilar, G., et al. 2018, *ApJS*, 235, 42
 Amorisco, N. C., Evans, N. W., & van de Ven, G. 2014, *Nature*, 507, 335
 Arp, H. 1966, *ApJS*, 14, 1
 Bender, R., Doebereiner, S., & Moellenhoff, C. 1988, *A&AS*, 74, 385
 Bender, R. & Moellenhoff, C. 1987, *A&A*, 177, 71
 Bender, R., Surma, P., Doebereiner, S., Moellenhoff, C., & Madejsky, R. 1989, *A&A*, 217, 35
 Bertin, E. & Arnouts, S. 1996, *A&AS*, 117, 393
 Bianchi, L. & GALEX Team. 2000, *Mem. Soc. Astron. Italiana*, 71, 1117
 Bidaran, B., Pasquali, A., Lisker, T., et al. 2020, *MNRAS*, 497, 1904
 Binggeli, B., Sandage, A., & Tammann, G. A. 1985, *AJ*, 90, 1681
 Bournaud, F., Jog, C. J., & Combes, F. 2005, *A&A*, 437, 69
 Brosch, N., Kaspi, S., Niv, S., & Manulis, I. 2015, *Ap&SS*, 359, 9
 Byrd, G. & Valtonen, M. 1990, *ApJ*, 350, 89
 Byun, W., Sheen, Y.-K., Park, H. S., et al. 2020, *ApJ*, 891, 18
 Cardelli, J. A., Clayton, G. C., & Mathis, J. S. 1989, *ApJ*, 345, 245
 Carter, D. 1978, *MNRAS*, 182, 797
 Carter, D. 1987, *ApJ*, 312, 514
 Casey, K. J., Greco, J. P., Peter, A. H. G., & Davis, A. B. 2023, *MNRAS*
 Chiboucas, K., Karachentsev, I. D., & Tully, R. B. 2009, *AJ*, 137, 3009
 Collins, M. L. M., Tollerud, E. J., Rich, R. M., et al. 2020, *MNRAS*, 491, 3496
 Côté, P., Mateo, M., Olszewski, E. W., & Cook, K. H. 1999, *ApJ*, 526, 147
 de Vaucouleurs, G. 1959, *Handbuch der Physik*, 53, 275
 Duc, P.-A., Cuillandre, J.-C., Karabal, E., et al. 2015, *MNRAS*, 446, 120
 Forbes, D. A., Cortesi, A., Pota, V., et al. 2012, *MNRAS*, 426, 975
 Forbes, D. A., Spitler, L. R., Graham, A. W., et al. 2011, *MNRAS*, 413, 2665
 Fried, J. W. & Illingworth, G. D. 1994, *AJ*, 107, 992
 Gil de Paz, A., Boissier, S., Madore, B. F., et al. 2007, *ApJS*, 173, 185
 Graham, A. W., Spitler, L. R., Forbes, D. A., et al. 2012, *ApJ*, 750, 121
 Hao, C. N., Mao, S., Deng, Z. G., Xia, X. Y., & Wu, H. 2006, *MNRAS*, 370, 1339
 Hubble, E. P. 1926, *ApJ*, 64, 321
 Jedrzejewski, R. I. 1987, *MNRAS*, 226, 747
 Kim, D.-W. 1989, *ApJ*, 346, 653
 Koch, A. 2009, *Astronomische Nachrichten*, 330, 675
 Koch, A., Black, C. S., Rich, R. M., et al. 2017, *Astronomische Nachrichten*, 338, 503
 Koch, A., Burkert, A., Rich, R. M., et al. 2012, *ApJ*, 755, L13
 Kroupa, P. 2001, *MNRAS*, 322, 231
 Lang, D., Hogg, D. W., Mierle, K., Blanton, M., & Roweis, S. 2010, *AJ*, 139, 1782
 McConnachie, A. W. 2012, *AJ*, 144, 4
 McWilliam, A. & Zoccali, M. 2010, *ApJ*, 724, 1491
 Morrissey, P., Conrow, T., Barlow, T. A., et al. 2007, *ApJS*, 173, 682
 Muñoz, R. P., Eigenthaler, P., Puzia, T. H., et al. 2015, *ApJ*, 813, L15
 Müller, O., Jerjen, H., & Binggeli, B. 2015, *A&A*, 583, A79
 Park, H. S., Moon, D.-S., Zaritsky, D., et al. 2017, *ApJ*, 848, 19
 Pasquali, A., van den Bosch, F. C., & Rix, H. W. 2007, *ApJ*, 664, 738
 Pastorello, N., Forbes, D. A., Foster, C., et al. 2014, *MNRAS*, 442, 1003
 Peng, C. Y., Ho, L. C., Impey, C. D., & Rix, H.-W. 2002, *AJ*, 124, 266
 Pulsoni, C., Gerhard, O., Arnaboldi, M., et al. 2018, *A&A*, 618, A94
 Rembold, S. B., Pastoriza, M. G., & Bruzual, G. 2005, *A&A*, 436, 57
 Rich, R. M., Collins, M. L. M., Black, C. M., et al. 2012, *Nature*, 482, 192
 Rich, R. M., Mosenkov, A., Lee-Saunders, H., et al. 2019, *MNRAS*, 490, 1539
 Schlafly, E. F. & Finkbeiner, D. P. 2011, *ApJ*, 737, 103
 Tal, T., van Dokkum, P. G., Nelan, J., & Bezanson, R. 2009, *AJ*, 138, 1417
 Torrealba, G., Belokurov, V., Kuposov, S. E., et al. 2019, *MNRAS*, 488, 2743
 Vazdekis, A., Koleva, M., Ricciardelli, E., Röck, B., & Falcón-Barroso, J. 2016, *MNRAS*, 463, 3409
 Zanatta, E. J. B., Cortesi, A., Chies-Santos, A. L., et al. 2018, *MNRAS*, 479, 5124